

1 Sorption Phenomena In Transient Vapor Intrusion
2 Scenarios

3 Jonathan G. V. Ström^a, Shuai Xie^a, Eric M. Suuberg^a

4 *These authors contributed equally to this work*

5 ^a*Brown University, School of Engineering, Providence, RI, USA*

6 **Abstract**

Abstract here

7 *Keywords:* Vapor intrusion, Temporal variability, Sorption, Attenuation
8 factor

9 **1. Introduction**

10 Many vapor intrusion (VI) contaminants has the capacity to sorb onto soil
11 and various common indoor materials, but the role and more importantly,
12 the consequences of these sorption processes in VI are poorly understood[1,
13 2, 3]. The migration of contaminant vapors from its source into the VI
14 affected building and potential indoor sources is usually the prime concern
15 in VI investigations. Rarely is the sorbed contaminant vapors in the soil
16 or indoor considered in an investigation, but these may potentially act as a
17 capacitor, storing and releasing contaminant vapors in response to a change in
18 contaminant concentration. Consequently, contaminant vapors may be much
19 more persistent at a site that has undergone remediation, potentially reducing
20 the effectiveness of mitigation systems, or impeding site investigations.

21 It is well recognized that building materials has the capacity to sorb pol-
22 lutants. The sorptive capacity of various volatile organic compounds (VOCs)
23 of concern in VI have been tested on a variety of building materials, such as
24 density board[4], gypsum wallboard[5], and plywood and carpets[6]. How-
25 ever, most of these studies used relative high contaminant concentrations,
26 usually around mg/m³[4] or even higher. This is several magnitudes higher
27 than the concentrations relevant in VI and due to the non-linear nature of
28 sorption with respect to concentration, sorption studies at lower concentra-
29 tion are needed.

30 Most of the VOC sorption studies have also focused on the interaction be-
31 tween building materials and formaldehyde[5], toluene, and decane[6]. How-
32 ever, one of the contaminants of greatest concern in VI - trichloroethylene
33 (TCE), has not received likewise attention. This is despite the fact that sorb-
34 ing TCE (and other VOCs) on activated carbon is extensively used to treat
35 indoor air contaminant and their use with passive sorption tube samplers[7].

36 Over the years many VI sites have been investigated for their potential
37 exposure risk. Two well-known examples of these are the studies of a house
38 in Layton, Utah and one in Indianapolis, Indiana. Both of these sites were
39 outfitted with a wide variety of instrumentation to measure various metrics
40 such as contaminant concentration in interior, soil, and groundwater, as well
41 as things like pressure, temperature, or weather. These studies yielded some
42 of the richest VI datasets available and gave invaluable insights, in particular
43 in the application of CPM[8] and sub-slab depressurization (SSD) mitigation
44 systems[9, 10]. However, neither of these studies considered the role of sorp-
45 tion had at these sites.

46 The potential impact of sorption could perhaps be most significant in
47 the application of the controlled pressure method (CPM) and various mit-
48 igation schemes. The controlled pressure method is the forced over- and
49 depressurization of a building to max- and minimize the contaminant entry
50 into the building. This can help the investigator ascertain the worst-case VI
51 scenario and help identify potential indoor contaminant sources[11, 8]. How-
52 ever, if the building indoor materials has a large sorptive capacities, then de-
53 and sorption processes may significantly affect the indoor air contaminant
54 concentration. Likewise, a significant amount of sorbed material may be re-
55 leased from the interior over an unknown period of time after mitigating the
56 contaminant intrusion at a site[1, 2].

57 In the past VI models have been used to gain insight into VI when no
58 field or experimental data has been available. Previously examples of VI
59 modeling studies are the role of rainfall in VI[12], or drivers of temporal
60 variability in some of the aforementioned sites[13]. However, while many VI
61 models include a sorption term in the governing equation for contaminant
62 transport in soils, none have explored the role of sorption in VI in a transient
63 simulation. The reason for this is two-fold. First, there has been a general
64 lack of interest in sorption and VI thus far. Secondly, the vast majority of VI
65 modeling efforts and studies has focused on steady-state analyses of VI, and
66 sorption only affects soil contaminant transport in time-dependent scenarios.

67 To bridge this knowledge gap we will begin to explore the role of sorp-

tion in VI through a combined effort of experimental and simulation work. Sorption data of TCE on various cinderblock, drywall, wood, paper, carpet, and Appling soil will be measured in a fixed bed sorption experiment. These sorption data will be used to generate kinetic sorption parameters to be used in our three-dimensional finite element VI model. For this purpose we will consider a prototypical VI scenario where a free-standing house with a basement is overlying a homogenously contaminated groundwater source. Using this model we will investigate how the dynamic contaminant transport is affected in general by sorption, how indoor sorption materials affect indoor air concentration as the building's pressurization fluctuates and how indoor air concentration are affected by indoor materials following successful mitigation of the structure.

2. Methods

2.1. Experimental Setup

To study the dynamic sorption of TCE onto the selected building materials, we use a two-step process - one for sorption and one for desorption.

In the sorption process a 17 by 1 cm stainless steel column is filled with material. (Before filling the column, some of the materials had to be ground-up using a coffee grinder.) Using flow controllers, TCE is diluted in nitrogen gas to 1.12 ppb_v and flowed through the column at a rate of x, for a pre-selected time period. After the material has sorbed for the selected time, the column is detached and attached to the desorption system.

In the desorption system, the column is heated to 100 °C and pure nitrogen gas is flowed through the previous outlet side of the column - carrying the desorbed contaminant with it. The now contaminated nitrogen gas is then passed through a long circular pipe, allowing the gas to cool to room temperature, and flowing into a carbon-filled stainless steel sorption column. The sorption column is then desorbed into a gas-chromatograph fitted with an electron capture device according to the EPA TO-17 standard.

The TCE dynamic sorption process of different building materials were determined by use of a method schematically shown in Figure 1. This method involved a selected material contained in an adsorption column through which TCE-containing gas was passed, and subsequent thermal desorption and measurement of the total amount of adsorption. During the adsorption part of the process, stainless steel tubes were packed with building materials held in place by glass wool. The amount of building material normally held in the

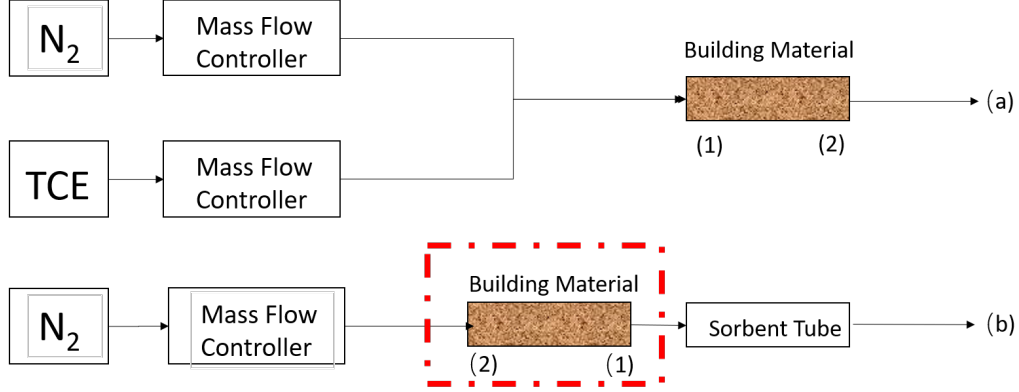


Figure 1: Schematic of experimental setup.

104 tube was around 1 g. It was determined that neither the glass wool nor the
 105 stainless steel tube would retain significant amounts of TCE. The sample-
 106 containing tubes were first exposed desired low concentrations of TCE in
 107 nitrogen, which were then allowed to interact with the flow for varying pe-
 108 riods of time. The typical flow rate of the nitrogen was 60 ml/min and the
 109 concentrations of TCE was around 1.1 ppbv. All of these adsorption experi-
 110 ments were conducted at room temperature. After a given time of exposure
 111 to the TCE-containing flow, that flow was stopped, and the sample tube
 112 was attached to a sorbent tube placed downstream of the sample tube. The
 113 sample tube was arranged such that the direction of the nitrogen flow in
 114 the subsequent desorption process was opposite that of the TCE-containing
 115 nitrogen flow during the adsorption process. During the thermal desorption
 116 step, the sample containing tube was covered by a heating mantle which per-
 117 mitted its heating at 100 °C. This allowed fully desorbing the TCE which
 118 had been held on the sample into a pure nitrogen flow, which carried it to
 119 the room temperature downstream sorbent tube, where it was again fully
 120 adsorbed. These tubes fully capture all of the TCE desorbed, from the sam-
 121 ples, and the amount of TCE was analyzed by Gas Chromatography (GC)
 122 with an Electron Capture Detector(ECD).

123 2.2. Numerical Model

124 To investigate the role of sorption in VI, we consider a simple VI scenario.
 125 Here we consider a house with a 10 by 10 m footprint, with the foundation
 126 bottom located 1 m below ground surface (bgs). The sole contaminant source
 127 is an uniformly TCE contaminated groundwater located 4 bgs, and the soil

Figure 2: The vapor intrusion model

128 surrounding the house is assumed to homogenous and of a singular type. All
129 contaminant vapors are assumed to enter the house through breaches in the
130 foundation, modeled as a 1 cm wide crack that runs along the perimeter of
131 the house. Finally we assume that sorption processes can occur both in the
132 soil matrix and in the indoor environment (on various indoor materials).

133 Modeling this scenario requires us to simulate a couple of physics, many
134 of which depend and interact with each other. The governing equations and
135 the physics they govern are:

- 136 1. van Genuchten retention model - soil moisture.
- 137 2. Darcy's Law - air flow in the porous media.
- 138 3. Transport equation - contaminant transport in porous media.
- 139 4. Continuously stirred tank reactor (CSTR) - contaminant concentration
140 in the indoor environment.

141 These physics are implemented in COMSOL Multiphysics, a commercial
142 finite-element method package, which is used to solve our model. It is impor-
143 tant to note that the indoor environment is implicitly modeled, but instead
144 only given by the CSTR equation; the soil domain is explicitly modeled.

145 2.2.1. Vadose Zone Moisture Content

146 Since the contaminant transport occurs through three-phased the vadose
147 zone, it is important that we correctly account for soil moisture content and
148 its effect on advective and diffusive transport. In this modeled scenario, we
149 assume that the soil moisture is at steady-state and does not change, and
150 thus the soil moisture content is given by the retention model developed by
151 van Genuchten.

The van Genuchten retention model gives the soil water saturation as a
function of elevation above groundwater. In turn this gives the water and

gas filled porosities, and the relative permeability of the soil matrix.

$$Se = \begin{cases} \frac{1}{(1+\alpha z^n)^m} & z < 0 \\ 1 & z \geq 0 \end{cases} \quad (1)$$

$$\theta_w = \begin{cases} \theta_r + Se(\theta_s - \theta_r) & z < 0 \\ \theta_s & z \geq 0 \end{cases} \quad (2)$$

$$k_r = \begin{cases} Se^l [1 - (1 - Se^{\frac{1}{m}})]^2 & z < 0 \\ 0 & z \geq 0 \end{cases} \quad (3)$$

152 Se is the saturation, and ranges from 0 to 1, which represent completely un-
 153 to fully saturated; z is the elevation above the groundwater in meters; θ_r ,
 154 θ_s , θ_w , and θ_g are the residual moisture content, saturated porosity (or just
 155 porosity), and water and air filled porosities respectively. All units are in
 156 volume of phase divided by the volume of soil; k_r is the relative permeability
 157 of water, which modifies the saturated permeability. This too ranges from 0
 158 to 1, indicating completely im- and permeable respectively. $1 - k_r$ gives the
 159 relative permeability of air.

160 2.2.2. Gas Flow In The Vadose Zone

161 The gas flow in the vadose zone is governed by a modified version of
 162 Darcy's Law. Originally, Darcy's Law was developed to describe flow in
 163 saturated porous media, but since we're interested in flow in unsaturated
 164 media, modification is necessary. An effective permeability that depends
 165 on the relative permeability from van Genuchten is introduced to allow for
 166 correct flow profiles in unsaturated porous media.

167 The vapor flow governing equation is given by

$$\frac{\partial}{\partial t}(\rho\theta_s) + \nabla \cdot \rho \left(- \frac{(1 - k_r)\kappa}{\mu} \nabla p \right) = 0 \quad (4)$$

168 Here ρ is the fluid density; ∇ is the del operator; κ is the saturated per-
 169 meability; μ is the fluid viscosity; and p is the fluid pressure. We assume
 170 that the contaminant vapors are so dilute that the gas flow properties can
 171 be taken to be those of air, and specifically at 20 °C and all the transport
 172 properties may be found in Table 1.

Boundary Conditions. To solve (4) we assign the atmosphere boundary (see Figure 2) to be at reference pressure and act as a gauge, i.e. zero pressure.

The foundation crack boundary is assigned the indoor-outdoor pressure difference value. Remaining boundaries are no-flow boundary conditions.

$$\text{Atmosphere} \quad p = 0 \text{ (Pa)} \quad (5)$$

$$\text{Foundation crack} \quad p = p_{\text{in/out}} \text{ (Pa)} \quad (6)$$

$$\text{All other} \quad -\vec{n} \cdot \rho_{\text{air}} \vec{u} = 0 \text{ (kg/(m}^2 \cdot \text{s))} \quad (7)$$

173 Here \vec{n} and \vec{u} are the boundary normal and gas velocity vectors.

174 *Initial Conditions.* For steady-state problems, the initial conditions don't
175 matter, but is simply zero for the entire domain. When solving transient,
176 the initial conditions are given by the steady-state solution.

177 2.2.3. Mass Transport In The Vadose Zone

178 Contaminants in the vadose zone exist in three phases - gaseous, solved in
179 water, and sorbed onto soil particles. While there are three distinct phases,
180 the water and gas phases are related via Henry's Law (8).

$$c_g = K_H c_w \quad (8)$$

181 Where c_g and c_w are the gas and water phase concentrations respectively in
182 mol/m³; K_H is the dimensionless Henry's Law constant.

183 In this work, we consider sorption between the soil and vapor phases, as
184 a function of the water contaminant concentration, through linear sorption
185 (9).

$$c_s = K_{\text{ads}} \rho_b c_g = K_{\text{ads}} \frac{\rho}{1 - \theta_t} K_H c_w \quad (9)$$

186 Here the c_s is the solid phase concentration in mol/kg; ρ_b is the bulk density
187 of the soil kg/m³, which is given by the density ρ and the total soil porosity
188 θ_t ; K_{ads} is the sorption isotherm in m³/kg. Using Henry's Law and the linear
189 isotherm we can express the total contaminant concentration in terms of the
190 water contaminant concentration.

191 Mass transport in the vadose zone is governed by diffusion and advection
192 and is given by (10).

$$R \frac{\partial c}{\partial t} = \nabla \cdot [D_{\text{eff}} \nabla c] - K_H \vec{u} \cdot \nabla c \quad (10)$$

193 The first term in (10) gives the change in contaminant water concentration
194 with respect to time, modified by the *retardation factor*, R , which is discussed

below; The second is the effective diffusive flux which is modified by the effective diffusion coefficient D_{eff} which is also discussed below. The third is the advective flux where \vec{u} is the soil-gas velocity from Darcy's Law, which when multiplied with K_H gives the gas phase concentration advective flux.

Contaminant entry into the building. The contaminant enters the building through a combination of advection and diffusive fluxes and is given by (11).

$$j_{ck} = \begin{cases} u_{ck}c_g - \frac{D_{\text{air}}}{L_{\text{slab}}}(c_{in} - c_g) & u_{ck} \geq 0 \\ u_{ck}c_{in} - \frac{D_{\text{air}}}{L_{\text{slab}}}(c_{in} - c_g) & u_{ck} < 0 \end{cases} \quad (11)$$

Here the j_{ck} is the molar contaminant flux into the building in $\text{mol}/(\text{m}^2 \cdot \text{s})$; D_{air} is the contaminant diffusion coefficient in pure air in m^2/s ; L_{slab} is the thickness of the foundation slab in m. The flux expression changes if there is a bulk flow into the building, i.e. $u_{ck} \geq 0$, or out of the building.

Retardation factor. As the contaminants are transported through the vadose zone, the partitioning between the various phases increases the contaminant residency time, retarding the transport of contaminants. This effect is represented by R which is the retardation factor (12).

$$R = \theta_w + \theta_g K_H + \rho_b K_H K_{\text{ads}} \quad (12)$$

Here θ_w , θ_g are the water and gas filled soil porosities; K_{ads} is the solid-gas phase sorption isotherm in m^3/kg . The diffusive and advective transport retardation is proportional to the inverse of R .

$$D_{\text{retarded}} = \frac{D_{\text{eff}}}{R} \quad (13)$$

$$\vec{u}_{\text{retarded}} = \frac{\vec{u}}{R} \quad (14)$$

It should be noted that the soil-gas velocity, \vec{u} , is not retarded in of itself, but rather just the contaminant being transported through advection, giving a effective bulk velocity.

Effective diffusivity. The effective diffusivity in the vadose zone varies with the soil moisture content, from being close to that in water when fully saturated and vice versa. Millington-Quirk developed (15) which describes the effective diffusivity in variably saturated porous media.

$$D_{\text{eff}} = D_{\text{water}} \frac{\theta_w^{\frac{7}{3}}}{\theta_t^2} + \frac{D_{\text{air}}}{K_H} \frac{\theta_g^{\frac{7}{3}}}{\theta_t^2} \quad (15)$$

216 Where the porosity fractions are the water and gas phase tortuosity terms;
 217 D_{air} and D_{water} are the contaminant diffusion coefficient in air and water
 218 respectively in m^2/s .

Boundary Conditions. A few boundary conditions are required to solve (10). In this model, the sole contaminant source is assumed to be the homogenously contaminated groundwater, which we assume to have a fixed concentration. The atmosphere acts as a contaminant sink, and any contaminant that makes it to this boundary is infinitely diluted, thus this is simply a zero concentration boundary condition. Contaminants leave the soil domain and enter the building through a combination of advective and diffusive gas phase transport. The last boundary condition is applied to all other boundaries and is a no-flow boundary.

$$\text{Groundwater} \quad c_w = 0 \text{ (mol/m}^3\text{)} \quad (16)$$

$$\text{Atmosphere} \quad c_w = c_{gw} \text{ (mol/m}^3\text{)} \quad (17)$$

$$\text{Foundation crack} \quad -\vec{n} \cdot \vec{N} = -\frac{j_{ck}}{K_H} \text{ (mol/(m}^2 \cdot \text{s))} \quad (18)$$

$$\text{All other} \quad -\vec{n} \cdot \vec{N} = 0 \text{ (mol/(m}^2 \cdot \text{s))} \quad (19)$$

219 $\vec{n} \cdot \vec{N}$ is the dot product between the boundary normal vector and the contaminant flux; j_{ck} is the contaminant vapor flux into the building. We assume
 220 that only contaminants in the gas phase enter the building, and dividing j_{ck}
 221 by K_H we get proper accounting in terms of the water phase concentration.
 222

223 *Initial Conditions.* For a steady-state condition the initial conditions don't
 224 matter, but are set to be zero everywhere. For transient simulations in this
 225 work, the steady-state solution is always used as an initial condition.

226 2.2.4. Indoor Environment

227 The indoor air space is modeled as a continuously stirred tank reactor
 228 (CSTR) given by (20). Contaminants are assumed to only enter through the
 229 foundation crack, represented by n_{ck} , which is calculated by integrating the
 230 contaminant flux over the foundation crack boundary. The product of air
 231 exchange rate, which govern how many house volumes are exchanged with
 232 the outside per time unit, and indoor air contaminant concentration gives the
 233 contaminant exit rate. The sorption of contaminant is given by the sorption
 234 reaction term in (22) and the sorbed contaminant concentration is given by
 235 (21).

Table 1: Transport properties and model parameters

$$V_{\text{bldg}} \frac{\partial c_{\text{in}}}{\partial t} = n_{\text{ck}} - A_e c_{\text{in}} V_{\text{bldg}} + r_{\text{sorb}} V_{\text{mat}} \quad (20)$$

$$V_{\text{mat}} \frac{\partial c_{\text{sorb}}}{\partial t} = -r_{\text{sorb}} V_{\text{mat}} \quad (21)$$

$$r_{\text{sorb}} = k_1 c_{\text{sorb}} - k_2 c_{\text{in}} \quad (22)$$

$$n_{\text{ck}} = \int_{A_{\text{ck}}} j_{\text{ck}} dA \quad (23)$$

Here V_{bldg} and V_{mat} are the indoor control volume and volume of indoor material in m^3 ; c_{in} and c_{sorb} are the indoor and sorbed (onto the indoor material) contaminant concentrations in mol/m^3 ; n_{entry} is the contaminant entry rate in mol/s , which is calculated by integrating the contaminant flux j_{ck} over the foundation crack area; r_{sorb} sorption rate in $\text{mol}/(\text{m}^3 \cdot \text{s})$; k_1 and k_2 are desorption and sorption reaction constants in $1/\text{s}$.

Fitting Kinetic Parameters. To calculate the indoor sorption rate we need k_1 and k_2 . These values are found by solving (22) numerically and then finding the best k_1 and k_2 by fitting them to the experimental data via least square. We use Runge-Kutta method of order 5(4) as the numerical solve, which is implemented together with the least square method in the SciPy python package[14].

3. Results & Discussion

3.1. Fitting Sorption Parameters

Using the numerical fitting scheme described in section 2.2.4 with the sorption data from the method described in section 2.1, the kinetic sorption parameters k_1 and k_2 are fitted. Figure 3 shows the result of this fitting and the sorption data for three select materials - wood, Appling soil, and cinderblock concrete. The k_1 and k_2 represent the rate at which TCE desorbs and sorbs respectively onto/from the material of interest. The equilibrium sorption constant is, using the formulation in (22), given by

$$K = \frac{k_1}{k_2} \quad (24)$$

and is used as the sorption isotherm. Here a small K indicate that there is a greater propensity for contaminant sorption.

To use the soil sorption isotherm in (10) K needs to be converted from being unitless to m^3/kg . This is done by multiplying the inverse of K isotherm with inverse of the soil bulk density ρ_b , which is taken to be $1460 \text{ kg}/\text{m}^3$.

$$K_{\text{ads}} = \frac{1}{K\rho_b} = 5.28 \text{ (m}^3/\text{kg)} \quad (25)$$

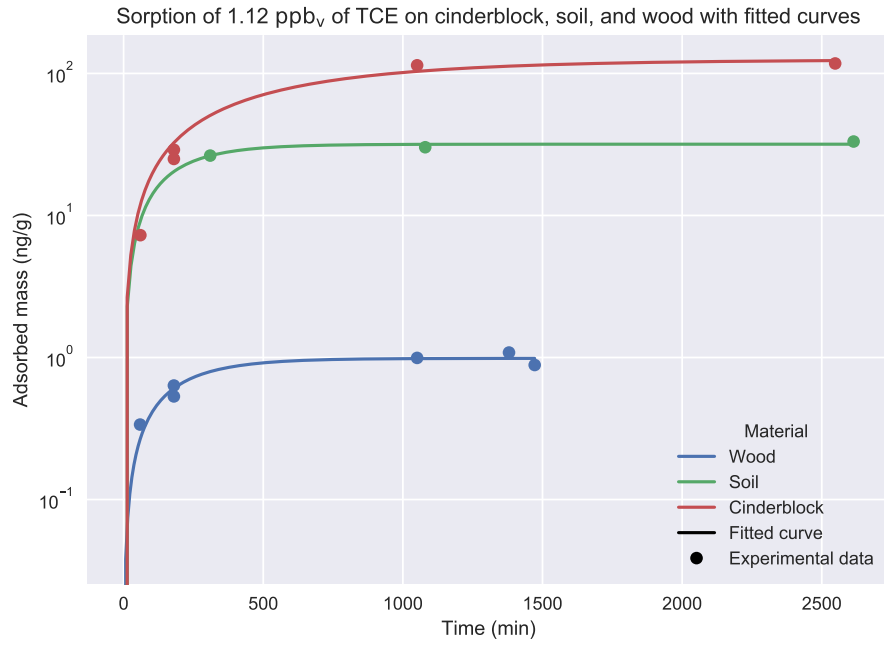


Figure 3: Experimental data of sorption of TCE onto three select materials as well as fitted sorption rates based on the kinetic model (22).

Table 2 shows the fitted parameters for the tested materials. Based on this these results we can see that cinderblock and soil have orders of magnitude larger sorption capacities than wood or drywall does. We can also see by the k_2 values that soil and cinderblock sorb quickly, much faster than a material with similar sorptive capacity such as paper.

Table 2: Fitted kinetic sorption parameters based on sorption experiment data.

Material	k_1 (1/hr)	k_2 (1/hr)	K
Wood	0.32	44.90	$7.10 \cdot 10^{-3}$
Drywall	0.41	87.94	$4.65 \cdot 10^{-3}$
Carpet	0.26	58.74	$4.42 \cdot 10^{-3}$
Paper	0.04	88.37	$4.55 \cdot 10^{-4}$
Soil	0.34	2636.57	$1.30 \cdot 10^{-4}$
Cinderblock	0.10	4175.16	$2.40 \cdot 10^{-5}$

267 3.2. Soil Sorption's Retarding Effect

Building pressurization is a key factor in VI that influences the advective contaminant transport. The magnitude of change in response to a pressurization change is significantly influenced by a range of factors, such as soil permeability, foundation depth, or soil moisture. To demonstrate the effect that soil sorption has on contaminant soil mass transport in the VI context, we run two types transient simulation where initially the modeled structure is at a steady -5 Pa, i.e. slightly depressurized. At the start of the simulation, the building building is 1) further depressurized to -15 Pa, or 2) overpressurized to 15 Pa, and the simulation is allowed to run for 72 hours.

$$\text{Depressurization : } \Delta p_{\text{in/out}} = \begin{cases} -5, & t = 0 \text{ (hr)} \\ -15, & 0 < t \leq 72 \text{ (hr)} \end{cases} \quad (26)$$

$$\text{Overpressurization : } \Delta p_{\text{in/out}} = \begin{cases} -5, & t = 0 \text{ (hr)} \\ 15, & 0 < t \leq 72 \text{ (hr)} \end{cases} \quad (27)$$

268 For each of these cases, the simulation is run using two different soil types
269 - sand and sandy loam. Sand is assumed here to not sorb any TCE, while
270 for sandy loam a range of sorption isotherms are used. These range from
271 no sorption ($K_{\text{ads}} = 0 \text{ (m}^3/\text{kg)}$) to the experimentally determined sorption
272 isotherm ($K_{\text{ads}} = 5.28 \text{ (m}^3/\text{kg)}$) in intervals multiplicative by 10^{-2} . With the
273 experimentally determined isotherm, we see that the ratio between sorbed
274 concentration and soil-gas phase concentration is 7708, i.e. there is a much
275 larger amount of sorbed contaminant. When $K_{\text{ads}} = 5.28 \cdot 10^{-4} \text{ (m}^3/\text{kg)}$ this
276 ratio is roughly unity (0.77), which is good to keep in mind in the following
277 discussion. These ranges of values can be used both to represent a soil that

278 has a smaller sorptive capacity or a situation where the sorbed and gas phase
 279 has not quite reached equilibrium.

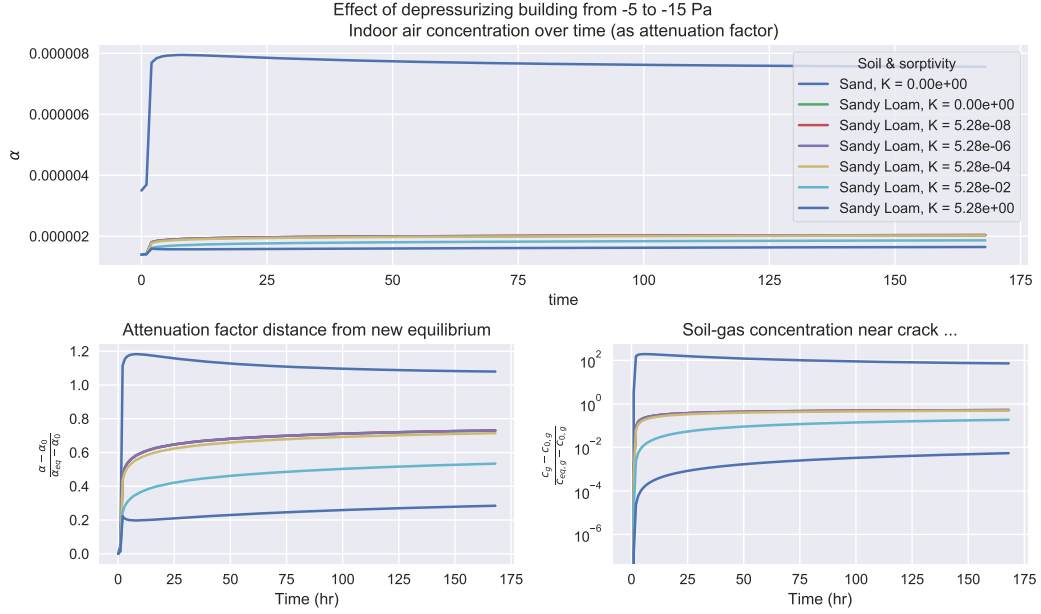


Figure 4

280 In the top panel of Figure 4, the indoor air contaminant concentration
 281 as the simulated building is undergoing the pressurization in (26) case. Here
 282 we can see that for the case when the surrounding soil consists of sand, the
 283 indoor concentration increases rapidly as the building is further pressurized.
 284 The rate of increase decreases significantly for the sandy loam cases, and
 285 progressively retards are the sorbed mass increases (K_{ads} increases).

286 The bottom left panel shows how far away the indoor air concentration (as
 287 attenuation factor) for each case is from reaching equilibrium. At the start
 288 of the simulation, the building starts with an attenuation of α_0 , which is the
 289 steady-state concentration when the building is pressurized with -5 Pa. As
 290 the building is further depressurized to -15 Pa, the indoor air concentration
 291 will approach a new equilibrium state α_{eq} (the result of which is from a
 292 steady-state simulation at that pressurization). By plotting $\frac{|\alpha - \alpha_0|}{|\alpha_{eq} - \alpha_0|}$ we can
 293 easily see how far away we are from the new equilibrium state, and a value
 294 of 0 represents that we are at the initial concentration, i.e. $\alpha = \alpha_0$, and a
 295 value of 1 represents $\alpha = \alpha_{eq}$.

296 This sort of analysis is applied to the bottom right panel as well, but
 297 instead of the indoor air concentration (as attenuation factor), we consider
 298 the average soil-gas concentration in a 5 cm diameter cylinder that envelop
 299 the entire perimeter crack. The choice of 5 cm is arbitrary, but helps illustrate
 300 what happens with the near-foundation-crack soil-gas concentration, changes
 301 in which allow us to better understand how the contaminant is transported
 302 into the building from the soil. The same could be done for the soil-gas
 303 velocity of course, but the rate of soil-gas velocity change is virtually the
 304 same for all of these cases, and reaches the new equilibrium velocity very
 305 quickly (much faster than the concentration) and is thus omitted from the
 306 figure.

307 Before discussing the role of sorption here, we can first compare the non-
 308 sorbing sand and sandy loam cases. Due to the higher permeability and
 309 lower moisture content, sand is significantly more permeable to gas flow than
 310 sandy loam (see Table 1 for permeability values). Consequently the advective
 311 transport through the foundation crack is much more significant, which is
 312 indicated by a Péclet number of around 4 versus 0.2 at a -15 Pa pressurization
 313 for sand and sandy loam respectively.

314 Due to the advection dominated transport mechanism in the sand case,
 315 the indoor air concentrations are temporarily elevated above the equilibrium
 316 concentration at -15 Pa, while the soil-gas concentration moves further away
 317 from equilibrium. (Note that the absolute distance from equilibrium is plot-
 318 ted in Figure 4 which is why at first glance one might think that the soil-gas
 319 concentration is two order of magnitude higher initially, but actually is two
 320 order of magnitude lower.) This phenomena occurs because initially more
 321 contaminants are drawn into the building from the near crack area than can
 322 be resupplied, temporarily depleting the local soil-gas contaminant concen-
 323 tration.

324 One can notice that many of the sandy loam lines overlap, and start
 325 diverging from each other when $K_{ads} = 5.28 \cdot 10^{-4}$ (m³/kg), at the point
 326 where the ratio of sorbed and soil-gas concentration are roughly equal. We
 327 see that this divergence occurs simultaneously in the indoor air and soil-
 328 gas contaminant concentration. However, since the indoor air concentration
 329 depend on the soil-gas concentration, we know that this is where the relevant
 330 difference is.

331 The simple reason for this is that it is at this threshold the sorptive
 332 contribution to the retardation factor (12) starts to becomes larger than the

333 other terms.

$$\rho_b K_H K_{\text{ads}} > \theta_w + \theta_g K_H \quad (28)$$

334 Thus it is at this point that the contaminant transport in the soil starts to
 335 become retarded by sorption. The physical reason for this is that the parti-
 336 tioning between the various phases gives a residence time as the contaminant
 337 is transported. Under VI conditions, the values of $\theta_w + \theta_g K_H$ are bounded to
 338 relatively small values, while K_{ads} can vary by orders of magnitude, making
 339 sorption potentially a very significant retarder for soil transport.

340 Figure 5 shows the same sort of analysis as in Figure 4 but with the
 341 building pressurization following (27). The results here are more or less the
 342 same, with the notable exception that in the sand case, the final equilibrium
 343 concentration is not initially exceeded. As the building is overpressurized,
 344 the indoor contaminant are pushed out into the soil. Since the indoor air con-
 345 centration is lower than the soil-gas concentration, this is entirely expected.

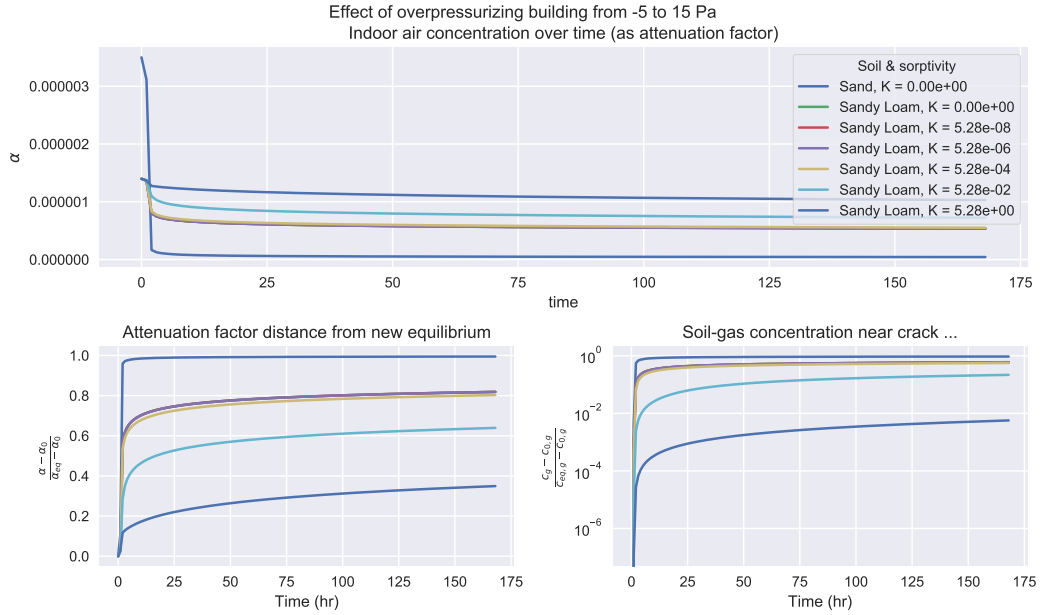


Figure 5

346 3.3. Indoor Material Sorption And Dynamics

347 We have now explored the effect that sorption has on contaminant mass
 348 transport in the sub-surface soil and seen its retarding effect. Now we turn

349 to exploring the effect of sorption onto/from various indoor materials has on
 350 the indoor air contaminant concentration. (Here we assume that there is no
 351 soil sorption.)

352 To study this we consider the basement (the indoor air space) and assume
 353 that the inside surfaces are entirely made up of one of the materials we studied
 354 in 3.1. We also assume that the material covering the indoor surfaces has
 355 a certain thickness or depth that the contaminants can penetrate - giving
 356 a certain volume or mass of sorbing material in the indoor. Table 3 shows
 357 the surface area, penetration depth, and volume of each material studied.
 358 While obviously some of these rooms are non-conventional and arbitrarily
 359 designed, i.e. you're unlikely to find a room with carpeted walls, floors, and
 360 ceiling, they do present some limiting cases of the potential effect of sorption
 361 onto/from these materials.

Material	d_p (mm)	V_{mat} (m ³)
Cinderblock	5	1.6
Wood	1	0.32
Drywall	10	3.2
Carpet	10	3.2
Paper	0.1	0.032

Table 3: The assumed contaminant penetration depth and subsequent volume of the sorbing indoor materials. The material surface area is assumed to be the same, and each material completely cover the surfaces of a 10x10x3 meter room.

362 The modeled building then undergoes a pressurization cycle, where at
 363 start of the simulation it is depressurized at -5 Pa and at steady-state. The
 364 building is then sequentially depressurized to -15 Pa, then pressurized to
 365 15 Pa, and finally again depressurized to -5 Pa. For each sequence, the
 366 new pressurization is maintained for 24 hours. This pressurization cycle
 367 may be seen in the top left panel of 6. The choice of pressurization cycle
 368 is somewhat arbitrary, but ours can be used to represent limiting cases of
 369 natural pressurization variation, or artificially induced pressurization. Figure
 370 6 shows the result of these simulations.

371 The change in indoor air contaminant concentration over this pressuriza-
 372 tion cycle is shown in the bottom panel of Figure 6. First we consider the
 373 reference case - where there is no sorbing indoor materials present. (The
 374 blue line is the reference case, which may be difficult to see as the wood and

375 carpet lines overlap.) Here we see that as the building is depressurized, the
 376 indoor air contaminant concentration increases quickly in response to the
 377 pressurization change, and is approaching an equilibrium.

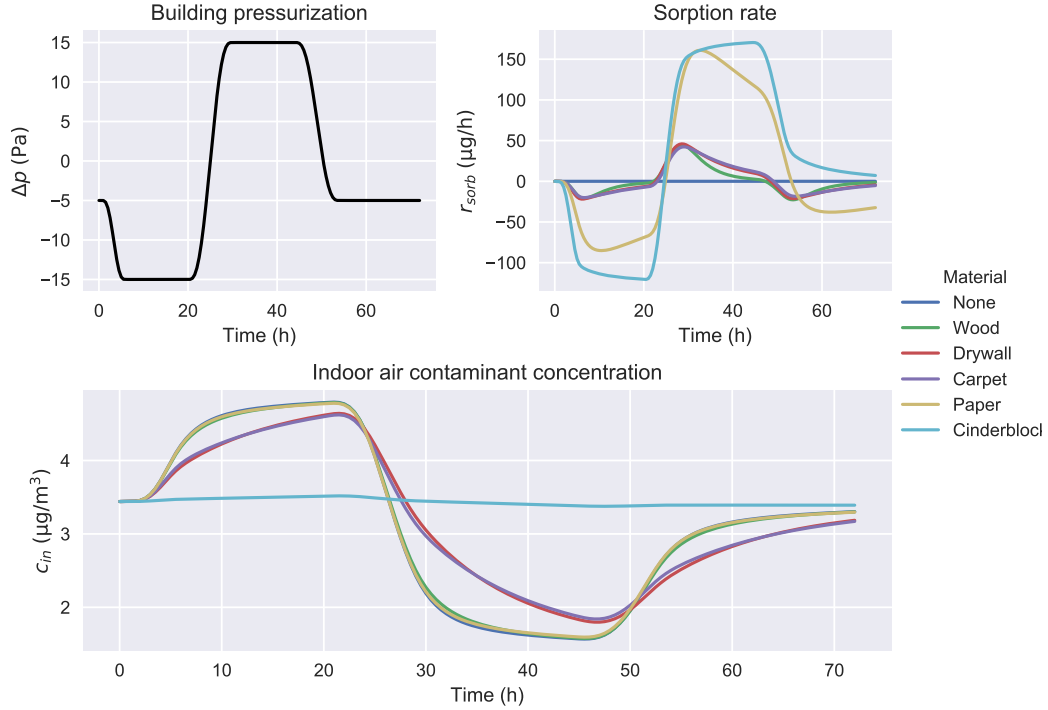


Figure 6: Comparison of how sorption onto/from various indoor materials affect the indoor air contaminant concentration (bottom) of a building that undergoes a pressurization cycle (top left). The rate of de- and sorption for each considered material during the cycle are also shown (top right) and is governed by (22).

378 By observation we can see that the presence of the various studied build-
 379 ing materials in the indoor environment has a very different effect on the
 380 change in indoor air contaminant concentration. The presence of wood and
 381 carpet has close to no effect on the indoor air concentration. While cin-
 382 derblock has a very significant effect, preventing almost any change in in-
 383 door concentration. Drywall and carpet is in the middle significantly delays
 384 the rate of change in the indoor concentration, but for each 24 hour cycle,
 385 roughly the same indoor concentration is reached as the reference case.

386 The disparity of these result is explained by the the top right panel of
 387 Figure 6. Here the de- and sorption rates in $\mu\text{g}/\text{hr}$ for each considered indoor

388 material is shown. A positive and negative value here indicate that contami-
 389 nant is desorbed respectively sorbed to and from the material. To understand
 390 this figure, it is useful to refer back to Table 2 which show the sorption and
 391 desorption rate constant k_1 and k_2 respectively, and the sorption equilibrium
 392 constant K (a smaller value indicate a larger sorptive capacity).

393 First we consider to the depressurization part of the cycle (1-25 hours).
 394 (Here see that the reference case has no sorption at all, by definition.) And
 395 similar to the indoor concentration panel, we see that the wood, drywall,
 396 and carpet cases overlap. This is explained by these materials have simi-
 397 lar sorptive capacities (K) and sorptive rates (k_2). Paper by contrast has
 398 a similar shape to the three previously mentioned, while the magnitude is
 399 significantly larger. This is because the K value for paper is one order of
 400 magnitude larger, indicating that wood, drywall, and carpet saturate with
 401 contaminant vapors over the time period, while paper does not. Cinderblock
 402 has a further order of magnitude larger K value, thus is even further away
 403 from being saturated, which explains the even faster sorption rate.

404 Next we consider the overpressurization period (25-49 hours). Again we
 405 see here that wood, drywall, and carpet behave the similarly for the same
 406 reasons as before, i.e. the desorption rate constants k_1 and sorption equilib-
 407 rium constants K are similar. This means that these reach the new sorbed
 408 contaminant saturation at roughly the same time.

409 Here it is important to note that due to the diffusion dominated transport
 410 through the foundation crack, even though the building is overpressurized,
 411 there is substantial contaminant entry. And because the sole contaminant
 412 source is the modeled contaminated groundwater, the sorbed equilibrium is
 413 relative to this entry rate.

414 Paper and cinderblock initially behave very similarly during the overpres-
 415 surization period and desorb contaminants quickly. However, paper reaches
 416 its saturation limit after a relatively short time, while cinderblock has not
 417 even at the end of the overpressurization cycle. Since the desorption rate
 418 constants k_2 are relatively similar for the materials, thus this disparity is
 419 primarily due to the different sorption equilibrium constants K .

420 Lastly, we consider the final period where the pressurization goes back
 421 to its initial state (49-72 hrs). Here we see that the reference case does
 422 not quite return to the initial indoor concentration. Thus the contaminant
 423 entry rate has not equilibrated yet, due to the soil contaminant concentration
 424 has not done so either. Like in the previous analysis we again see that
 425 the wood, drywall, and carpet cases don't differ from the reference. The

paper case is slightly more different, but for the same reasons that have already been discussed. Cinderblock is unique here though, as we clearly see that it is releasing contaminants, due to the previous change in contaminant concentration has been so significantly retarded.

From this simulation work we can see how varied the effect of sorbing indoor materials are. Most of the tested materials only have a moderate effect on the indoor air contaminant concentration dynamics, with the notable exception of cinderblock, which effectively enforces a pseudo-steady-state. However we also see from the analysis of the sorption dynamics that the desorption and sorption rate constants k_1 and k_2 are less important than the sorptive capacity K of the material.

3.4. Indoor Material Sorption And Mitigation

The work done by us and others have shown the large sorptive capacities of various common materials. The desorption of the sorbed contaminants may have significant impact on the efficacy of various mitigation systems. To investigate this we turn to our model and consider a scenario where initially the modeled building is depressurized with -5 Pa and at the start of the simulation some perfect mitigation scheme is turned on and the contaminant entry n_{entry} in (??) goes to zero. We also assume that for each case, the indoor environment contains the same amount of indoor material as described in section 3.3. The air exchange rate is assumed to remain a constant 0.5 per hour for the entire 72 hour simulation time.

The decrease in indoor air concentration (as attenuation factor α) for each simulated case is seen in Figure 7. As expected, when there is no sorbing indoor materials, i.e. our reference case, the indoor concentration decreases log-linearly. We can also see that the contaminant desorption from the materials maintain a higher indoor air concentration relative to reference, with cinderblock again shown to have the great impact.

4. Conclusions

Acknowledgements

This project was supported by grant ES-201502 from the Strategic Environmental Research and Development Program and Environmental Security Technology Certification Program (SERDP-ESTCP).

Declaration of interest: none

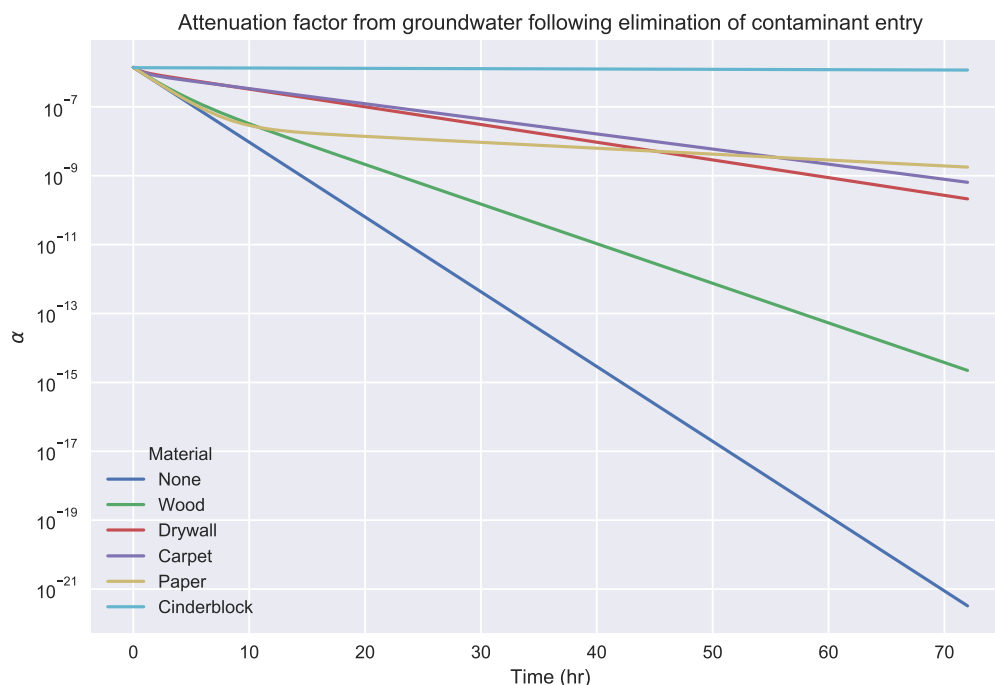


Figure 7

References

- [1] R. Meininghaus, L. Gunnarsen, H. N. Knudsen, Diffusion and Sorption of Volatile Organic Compounds in Building Materials-Impact on Indoor Air Quality, *Environ. Sci. Technol.* 34 (15) (2000) 3101–3108. doi:10.1021/es991291i.
- [2] R. Meininghaus, E. Uhde, Diffusion studies of VOC mixtures in a building material, *Indoor Air* 12 (4) (2002) 215–222. doi:10.1034/j.1600-0668.2002.01131.x.
- [3] F. D. Tillman, J. W. Weaver, Review of Recent Research on Vapor Intrusion (2005) 47.
- [4] X. Wang, Y. Zhang, J. Xiong, Correlation between the solid/air partition coefficient and liquid molar volume for VOCs in building materials, *Atmospheric Environment* 42 (33) (2008) 7768–7774. doi:10.1016/j.atmosenv.2008.05.030.

- 474 [5] J. Xu, J. S. Zhang, X. Liu, Z. Gao, Determination of partition and
475 diffusion coefficients of formaldehyde in selected building materials and
476 impact of relative humidity, *J. Air Waste Manag. Assoc.* 62 (6) (2012)
477 671–679. doi:10.1080/10962247.2012.665812.
- 478 [6] A. Bodalal, J. S. Zhang, E. G. Plett, A method for measuring internal
479 diffusion and equilibrium partition coefficients of volatile organic com-
480 pounds for building materials, *Building and Environment* 35 (2) (2000)
481 101–110. doi:10.1016/S0360-1323(99)00005-0.
- 482 [7] U.S. Environmental Protection Agency, OSWER Technical Guide for
483 Assessing and Mitigating the Vapor Intrusion Pathway From Subsurface
484 Vapor Sources To Indoor Air (2015).
- 485 [8] C. Holton, Y. Guo, H. Luo, P. Dahlen, K. Gorder, E. Dettenmaier,
486 P. C. Johnson, Long-Term Evaluation of the Controlled Pressure Method
487 for Assessment of the Vapor Intrusion Pathway, *Environ. Sci. Technol.*
488 49 (4) (2015) 2091–2098. doi:10/f64j45.
- 489 [9] C. C. Lutes, R. S. Truesdale, B. W. Cosky, J. H. Zimmerman,
490 B. A. Schumacher, Comparing Vapor Intrusion Mitigation System
491 Performance for VOCs and Radon, *Remediation* 25 (4) (2015) 7–26.
492 doi:10/gd6dfn.
- 493 [10] U.S. Environmental Protection Agency, Assessment of Mitigation Sys-
494 tems on Vapor Intrusion: Temporal Trends, Attenuation Factors, and
495 Contaminant Migration Routes under Mitigated And Non-mitigated
496 Conditions (2015).
- 497 [11] T. McHugh, P. Loll, B. Eklund, Recent advances in vapor intrusion
498 site investigations, *Journal of Environmental Management* 204 (2017)
499 783–792. doi:10/gd6dgk.
- 500 [12] R. Shen, K. G. Pennell, E. M. Suuberg, A numerical investigation of
501 vapor intrusion — The dynamic response of contaminant vapors to
502 rainfall events, *Science of The Total Environment* 437 (2012) 110–120.
503 doi:10/f4fp9s.
- 504 [13] J. G. V. Ström, Y. Guo, Y. Yao, E. M. Suuberg, Factors affect-
505 ing temporal variations in vapor intrusion-induced indoor air contam-

- 506 inant concentrations, Building and Environment 161 (2019) 106196.
507 doi:10.1016/j.buildenv.2019.106196.
- 508 [14] E. Jones, T. Oliphant, Pearu Peterson, SciPy: Open source scientific
509 tools for Python (2011).